Large-Area Monolayer Hexagonal Boron Nitride on Pt Foil

Ji-Hoon Park,[†,‡] Jin Cheol Park,[‡,§] Seok Joon Yun,[‡,§] Hyun Kim,[‡,§] Dinh Hoa Luong,[‡,§] Soo Min Kim,[⊥] Soo Ho Choi,[∥] Woochul Yang,[∥] Jing Kong,[#] Ki Kang Kim,[†,*] and Young Hee Lee[‡,§,*]

[†]Department of Energy and Materials Engineering and Advanced Energy and Electronic Materials Research Center (AEEMRC), Dongguk University—Seoul, Seoul 100-715, Republic of Korea, [‡]Center for Integrated Nanostructure Physics, Institute for Basic Science, Sungkyunkwan University, Suwon 440-746, Republic of Korea, [§]Departments of Energy Science and Physics, Sungkyunkwan University, Suwon 440-746, Republic of Korea, [⊥]Institute of Advanced Composite Materials, Korea Institute of Science and Technology (KIST), Jeollabuk-Do 565-902, Republic of Korea, [∥]Department of Physics, Dongguk University—Seoul, Seoul 100-715, Republic of Korea, and [#]Department of Electrical Engineering and Computer Sciences, Massachusetts Institute of Technology, Cambridge, Massachusetts 02139, United States

ABSTRACT Hexagonal boron nitride (h-BN) has recently been in the spotlight due to its numerous applications including its being an ideal substrate for two-dimensional electronics, a tunneling material for vertical tunneling devices, and a growth template for heterostructures. However, to obtain a large area of h-BN film while maintaining uniform thickness is still challenging and has not been realized. Here, we report the systematical study of h-BN growth on Pt foil by using low pressure chemical vapor deposition with a borazine source. The monolayer h-BN film was obtained over the whole Pt foil (2×5 cm^2) under <100 mTorr, where the size is limited only by the Pt foil size. A borazine source was catalytically decomposed on the Pt surface, leading to the self-limiting growth of the monolayer without the associating precipitation, which is very similar to the growth of graphene on Cu. The orientation of the h-BN domains was largely confined by the Pt domain, which is confirmed by polarizing optical microscopy (POM) assisted by the nematic liquid crystal (LC) film. The total pressure and orientation of the Pt lattice plane are crucial parameters for thickness control. At high pressure (~0.5 Torr), thick film was grown on Pt (111), and in contrast, thin film was grown on Pt (001). Our advances in monolayer h-BN growth will play an important role to further develop a high quality h-BN film that can be used for vertical tunneling, optoelectronic devices and growth templates for a variety of heterostructures.

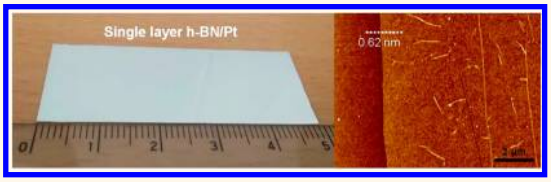

KEYWORDS: hexagonal boron nitride · chemical vapor deposition · borazine · platinum foil · nematic liquid crystal

Two-dimensional hexagonal boron nitride (h-BN), a honeycomb lattice with strong ionic bonding of boron and nitrogen atoms, is the thinnest insulating nanomaterial with an electrical band gap of 5.9 eV.[1] It has been used as a substrate to improve the electrical properties of graphene devices.[2,3] Since the surface of h-BN is atomically smooth and free of dangling bonds, charge scattering of graphene has been reduced so that the mobility of graphene devices on an h-BN substrate is almost an order of magnitude higher than that of devices on a SiO_2/Si substrate. In addition, h-BN can be applied to an ideal substrate for growing graphene epitaxially, due to the small lattice mismatch of about 1.7%.[4] Theoretical calculation suggests that the graphene on an h-BN substrate opens the band gap because of the local potential variation for bond distortion and moiré periodicity.[5,6] Furthermore, it poses high mechanical, chemical, and temperature stability, as well as high thermal conductivity.[7−9] It has also been used as a membrane for strong oxidation resistance, h-BN resin as inorganic filler and thermal dissipation in devices.[10−12]

To synthesize monolayer h-BN, ultra-high vacuum chemical vapor deposition (UHVCVD) has been employed with a borazine precursor on single-crystalline transition metals such as Ni,[13,14] Pt,[15] Pd,[16] Rh,[17,18] Ag,[19,20] and *etc.* UHVCVD equipped with low energy-electron diffraction, high resolution electron energy loss spectroscopy, angle-resolved ultraviolet photoelectron spectroscopy, X-ray photoelectron spectroscopy, X-ray photoelectron diffraction, and scanning tunneling microscopy measurements is helpful to study the growth mechanism, the interaction between h-BN and substrate, and/or the electronic band structure of h-BN, whereas it is difficult to scale up for mass production with a large area of h-BN.[21] To overcome the limitation, an alternative method is

* Address correspondence to kkkim@dongguk.edu, leeyoung@skku.edu.

Received for review June 10, 2014 and accepted August 5, 2014.

Published online August 05, 2014
10.1021/nn503140y

required. Inspired by graphene synthesis on polycrystalline copper foil by using chemical vapor deposition (CVD), the growth of large-area h-BN has been carried out on various polycrystalline catalytic substrates such as Ni,[22−24] Co,[25,26] Cu,[27−30] and Pt[31,32] foils or on their thin films. When Ni foil was used as a growth substrate, the thickness of h-BN varied depending on the Ni surface orientation due to the different catalytic activities. Therefore, while thick h-BN was grown on Ni (100) surface, h-BN was not grown on Ni (111) surface.[23] The exact growth mechanism is still unclear at this moment. Monolayer or bilayer patched h-BN was synthesized on Co (111) thin film, but the surface morphology strongly affects the formation of monolayer h-BN; that is, the multilayer h-BN was grown on the rough surface due to the precipitation of the B and N atoms at the Co grain boundaries.[26]

Large area h-BN has been synthesized on Cu foil.[27,28] However, the mechanical strength of the h-BN film obtained from the indentation measurement using AFM tip was not as high as the theoretical value, which was attributed to reduced stiffness due to vacancy defects in the h-BN film.[27] Recently, monolayer or bilayer h-BN synthesized on Pt foil was observed as being of high quality, with the thickness of h-BN being able to be controlled by the amount of ammonia borane as a new precursor.[31,32] However, the underlying growth mechanism related to Pt lattice orientation and pressure is far from being clearly understood. In addition, the size of polycrystalline h-BN domains is still unknown when h-BN is grown under different growth conditions. For this purpose, a facile method of observing the h-BN domain size is further required.

As mentioned above, the solid precursor of ammonia borane has been widely used for h-BN growth, with ammonia borane being thermally decomposed into hydrogen, borazine, and polymeric aminoborane as precursors.[28] Yet, it is not easy to control the amount of precursors by heating temperature or its weight. The accumulation of precursors at a lower temperature region through the gas line and the deposition of unwanted onion-like BN particles is caused by thermally activated polymeric aminoborane.[28,30] A filter was used to remove the polymeric aminoborane, which was installed between the chamber and the ammonia borane lines[30,32] but it was still difficult to remove it completely.

In this work, we report the systematic study for synthesizing large-area monolayer h-BN film on polycrystalline Pt foil by using borazine as a precursor at low pressure chemical vapor deposition (LPCVD). The advantage of the borazine source compared to the ammonia borane is discussed. The effect of the Pt lattice orientation, the total pressure, and the different cooling rate on h-BN growth is examined further to understand the growth mechanism. Furthermore, the liquid crystal (LC)-assisted polarizing optical microscopy

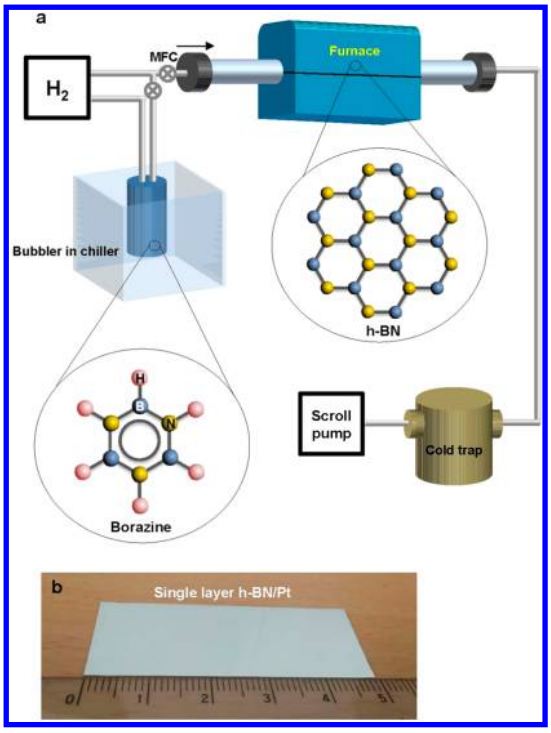

Figure 1. (a) The schematic diagram of LPCVD equipped with a bubbler using liquid borazine precursor and a cold trap to prevent the damage of the scroll pump. (b) Photography of h-BN on Pt foil with a size of 2 × 5 cm^2.

(POM) method was used to visualize the size and orientation of h-BN domains. We found that large-area monolayer polycrystalline h-BN was grown by the self-limiting surface growth mechanism under optimized growth conditions regardless of the Pt orientation. The orientation and size of h-BN grains were largely affected by the orientation of the Pt domain, but misaligned h-BN intra-domains within the h-BN grains were also found.

RESULT AND DISCUSSION

Figure 1a shows the schematic diagram of LPCVD equipped with a bubbler for the liquid-phase borazine source. The bubbler filled with liquid borazine was kept at a temperature of −10 °C in a chiller to avoid the self-decomposition of the borazine. Hydrogen was used as the carrier gas to supply the vaporized borazine into the chamber. A cold trap was installed to prevent the damage of the scroll pump. Figure 1b presents the h-BN on a Pt foil with a size of 2 × 5 cm^2. The borazine source is advantageous over ammonia borane since the solid precursor, ammonia borane, accumulates in the chamber at low temperatures, which leads to the deposition of unwanted BN particles by thermal activation during growth.[28] Therefore, ammonia borane is not an ideal precursor for growth (see Supporting Information, Figure S1).

Figure 2a shows the scanning electron microscopy (SEM) image of as-grown h-BN film on Pt foil. The h-BN wrinkles caused by the thermal expansion coefficient difference during cooling were clearly observed on the

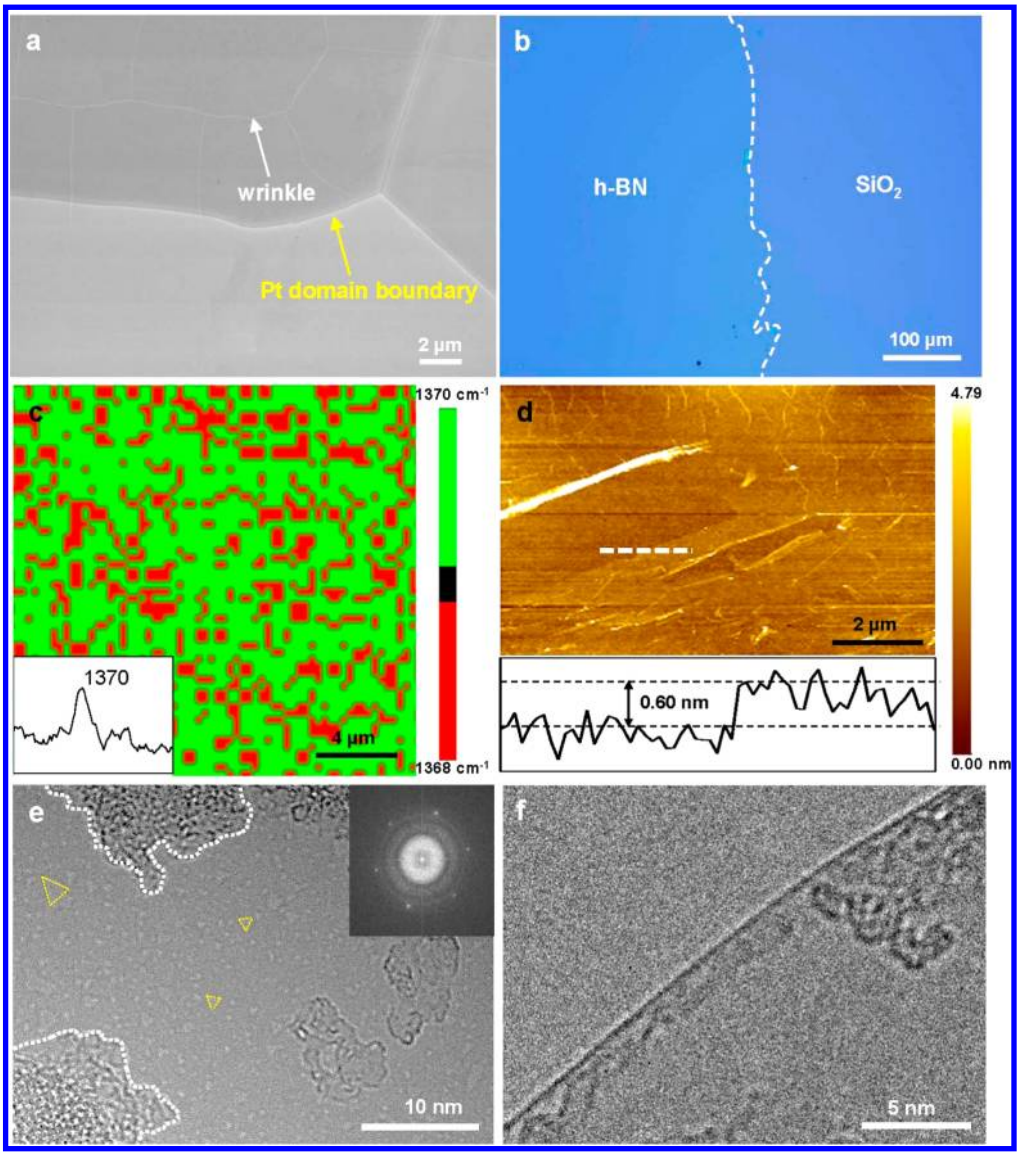

Figure 2. Characterization of monolayer h-BN. (a) SEM image of h-BN on Pt foil. The white and yellow arrows indicate the h-BN wrinkles and Pt domain boundary, respectively. (b) Optical image of h-BN transferred onto a 300 nm SiO_2/Si substrate by using the bubbling transfer technique. (c) Raman mapping image for the position of E_{2g} phonon mode of h-BN. Note that the maximum variance in the image is only 2 cm^{-1}. The inset shows the representative Raman spectra of monolayer h-BN. (d) AFM image of the h-BN on the SiO_2/Si substrate and the height profile along the white long-dashed line in (d). (e) Atomic-resolution TEM image of monolayer h-BN. The inset shows a selective diffraction pattern image. The yellow-dashed triangles indicate the triangle-shaped vacancy structure caused by the electron knock-on damage with an acceleration voltage of 80 kV during TEM observation. (f) TEM image of the basal plane (0001) for monolayer h-BN.

Pt surface. In addition, the h-BN wrinkles were extended across Pt grain boundaries, indicating that the h-BN film is uniformly grown over the entire region (see Supporting Information, Figure S2). After it was transferred onto a 300 nm SiO_2/Si substrate by using the bubble transfer technique,[31,32] the optical contrast of the h-BN film was quite uniform and practically undistinguishable from the SiO_2/Si substrate (Figure 2b). Only the torn h-BN film can be observed, indicating that the thickness of the h-BN is very thin and uniform. The existence of h-BN is further characterized by confocal Raman spectroscopy. Confocal Raman spectroscopy is very useful to analyze the thickness, quality, and uniformity of h-BN films.[3,33] Figure 2c shows the Raman mapping image for the position of the E_{2g} phonon mode (~1370 cm^{-1}) of h-BN and its inset presents the representative Raman spectra of the h-BN film. Compared to the E_{2g} position (~1366 cm^{-1}) for bulk h-BN, the E_{2g} position of the monolayer h-BN was blue-shifted and ranged from 1368 to 1370 cm^{-1}.[34,35] The fluctuation of the E_{2g} position was small and might be attributed to the local strain at the h-BN wrinkle.[34] Consequently, the monolayer h-BN grown here is structurally uniform over the entire region.

To understand the atomic structure of the h-BN film and measure its thickness, atomic force microscopy (AFM) and transmission electron microscopy (TEM) were used. The thickness of the h-BN film was

measured near the region of the torn h-BN film (created accidentally during transfer) by AFM, as shown in Figure 2d. The transferred h-BN still remained clean without additional particles, indicating that a borazine source is better than an ammonia borane source (see Supporting Information, Figure S1). The height profile in the inset of Figure 2d shows that the thickness of the h-BN film is around 0.6 nm, confirming that the obtained h-BN film is a monolayer. The TEM image in Figure 2e presents a monolayer h-BN region with some hydrocarbons (white-dashed lines), as confirmed by electron energy loss spectroscopy (EELS) (see Supporting Information, Figure S3). The h-BN bonds were sp^2-hybridized, as confirmed by the π^* and σ^* energy-loss peaks at the boron K-shell (near 180 eV) in the EELS spectra.[36] The atomic arrangement of hexagonal B and N atoms was not clearly observed due to the electron knock-on damage with an acceleration voltage of 80 kV during the TEM observations.[37] On the other hand, the triangle-shaped vacancy structures indicated by yellow-dashed triangles were frequently observed in the h-BN film, which is in agreement with previous observation for monolayer h-BN.[37] It has been reported that the displacement threshold energy (E_d) for B and N atoms in the pristine h-BN is approximately 80 and 120 kV, respectively. The E_d at the monovacancy edges for B/N is ~70 and 80 kV, respectively. The E_d for B/N at the edges of larger vacancies is further decreased. The asymmetry and reduction in the E_d for B/N, as the number of vacancies at the edge increases, are attributed to generate the triangle-shape vacancy structure and enlarge its size during the observation. However, the single hexagonal dot patterns in the FFT image corresponding to the whole h-BN monolayer image, as displayed in the inset of Figure 2e, is clearly observed, proving that the atomic arrangement of B and N is hexagonal and single-crystalline at the region of Figure 2e. The monolayer h-BN was confirmed by examining the folded edge of the layer in Figure 2f. In addition, the polycrystalline nature was frequently observed over large area (>30 μm^2), which was confirmed by comparing the tilted angle of the hexagonal spots in a selective area electron diffraction pattern (SAED) at the low magnification (see Supporting Information, Figure S3). The stoichiometry of boron and nitrogen was 1:1, as obtained by X-ray photoelectron spectroscopy (XPS) (see Supporting Information Figure, S4).

To understand the growth mechanism of h-BN on Pt foil, different cooling rates were applied. In the case of graphene growth on the catalytic substrate, whether the surface-mediated mechanism or the precipitation growth mechanism dominates is determined by the carbon solubility in the substrate at the growth temperature.[38] The solubility of carbon in copper is around 0.0001 atom %; therefore, graphene is only grown on the Cu surface, and the cooling rate does not affect the growth morphology.[39] However, the carbon solubility in Ni at the growth temperature of 1000 °C is around 1 atom % resulting in carbon precipitation onto the Ni surface during cooling.[40] As a consequence, graphene or thin-layer graphite is formed depending on the cooling rate and Ni lattice orientation. Pt has boron solubility of 1 atom % at a temperature of 1100 °C, with some Pt_3B or Pt_2B compound phases occurring at wider temperature ranges.[41] On the other hand, nitrogen is not soluble at all in Pt. Therefore, it is not clear whether h-BN is grown by surface-mediated or precipitation growth on Pt foil.

Figure 3 shows the results of different cooling rates of −171 °C/min and −5 °C/min from 1100 to 700 °C. In Figure 3, panels a and d show the SEM images of fast cooling and slow cooling, respectively. Interestingly, the big wrinkles were observed in the fast-cooled sample, whereas such big wrinkles were rarely observed in the slowly cooled sample. The wrinkle heights in the fast- and slow-cooled samples on Pt foil were 6.4 and 0.6 nm, respectively, as measured by AFM (Figure 3b,e). The thicknesses of the h-BN film of the fast-cooled and slow-cooled samples, after transfer onto 300 nm SiO_2/Si were 0.62 and 0.63 nm, respectively, indicate that the thicknesses of both films are quite similar to each other (Figure 3c,f). In addition, the thickness of the h-BN obtained from the medium cooling rate of −28 °C/min was 0.64 nm (see Supporting Information Figure S5). As a consequence, the cooling rate did not affect the thickness of the h-BN, assuring that the monolayer h-BN was formed by the surface-mediated growth mechanism. This result is similar to the growth mechanism for graphene or h-BN on Cu foil. Therefore, although there is boron solubility in the Pt bulk and the formation of Pt−B compounds at the growth temperature, the enthalpy of the h-BN phase could be lower than those of Pt−B compounds in the Pt bulk, leading to the growth of an h-BN film on the Pt surface. Detailed theoretical calculations would help to elucidate this mechanism in the future.

The schematic diagram of Figure 3g shows the plausible mechanism for different wrinkle heights. The thermal expansion coefficients of h-BN and Pt are -2.9×10^{-6} and 8.8×10^{-6} K^{-1} at room temperature.[42,43] Therefore, shrinkage is more dominant due to the higher thermal expansion coefficient of Pt in comparison to that of the h-BN.[28] As reported previously,[32] the interaction between h-BN and Pt is weak. However, it is possible to have a strong interaction between h-BN and Pt *via* Pt defects, some impurities, and Pt grain boundaries. The fast shrinkage of the Pt foil takes place during the fast cooling. The h-BN film might slip where there is weak interaction with the Pt foil. However, where the interaction between h-BN and Pt is strong, the film can adhere to the Pt surface, leading to the formation of big wrinkles, as shown in Figure 3g. On the

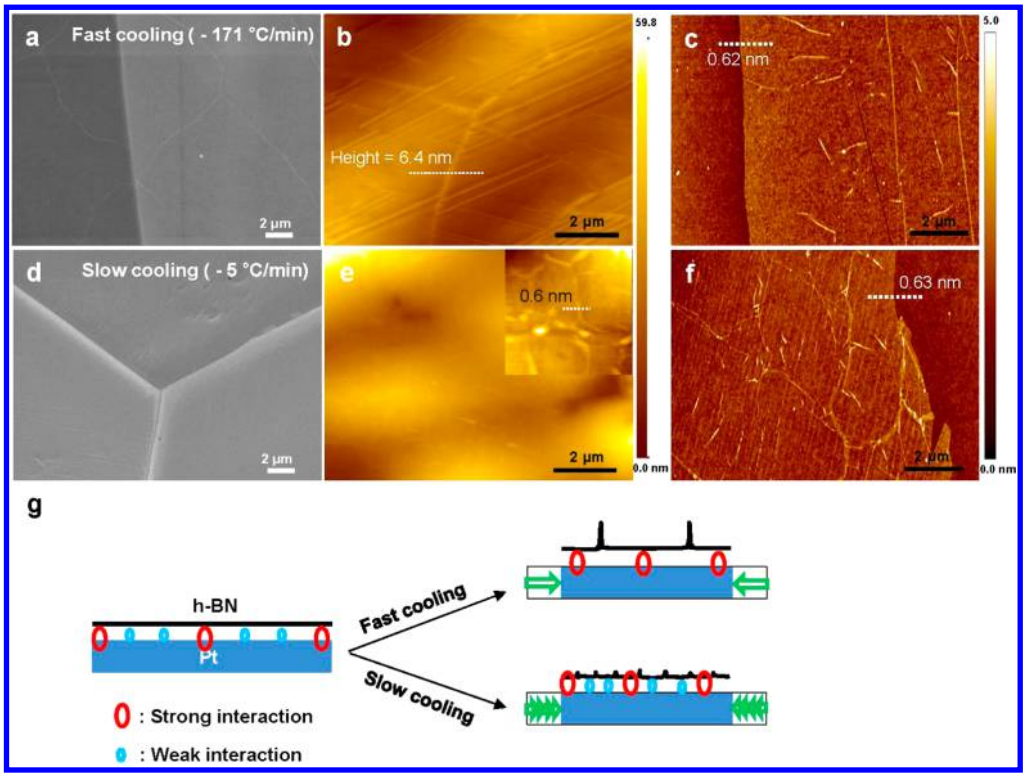

Figure 3. The effect of cooling rate. SEM images (a and d) and AFM morphologies (b, c, e, and f) for the fast (a−c) and slow (d−f) cooling rate of −171 °C and −5 °C/min from 1100 to 700 °C, respectively. The wrinkle heights are 6.4 and 0.6 nm, respectively. (c and f) AFM images of fast and slow cooled h-BN transferred onto the SiO_2/Si substrate, respectively. The step height between substrate and h-BN film along the white dotted line is 0.62 and 0.63 nm, respectively. (g) The schematic diagram of the possible mechanism for different winkle heights.

other hand, in the case of slow cooling, small wrinkles are formed locally without any slipping.

To understand the effect of Pt lattice orientation for h-BN growth, the grain orientation of the Pt foil after the h-BN growth is analyzed by using electron backscatter diffraction (EBSD) in SEM. Figure 4a,b shows the SEM image of the polycrystalline Pt surface and the EBSD mapping image with the EBSD legend for the same region. To match the same region, silver-paste marker was used. The size of the Pt domain ranged from 50 to 300 μm. To study the effect of lattice orientation in detail, the Pt (111) and Pt (001) planes were traced, as indicated by the white- and green-dotted lines in Figure 4a,b. Figure 4c shows the optical image of the Pt surface covered by an h-BN film. By comparing that with EBSD image, the Pt (111) and (001) planes indicated by the dotted lines were identified. Since the sample was tilted at an angle of 70 degree for EBSD measurement, the shape of the Pt domains were slightly different from SEM and optical images. After the h-BN film was transferred onto the 300 nm SiO_2/Si (Figure 4d), no trace of a Pt grain boundary was observed. The h-BN film was grown uniformly regardless of Pt lattice orientation.

To directly observe the size and orientation of the h-BN domain, the LC-assisted POM method was performed.[44,45] It has been reported that grain boundaries in graphene film can be visualized by using the self-alignment of LC along the graphene domain orientation anisotropically *via* $\pi-\pi$ stacking between graphene and LC. Since the h-BN is a hexagonal structure, with a similar lattice constant to graphene (2.504 Å (h-BN) and 2.456 Å (graphene)), it is anticipated that the similar texture of nematic LC on h-BN can be visualized with the same technique. Figure 4e shows the optical image of the LC-coated h-BN film on 300 nm SiO_2/Si with a silver-paste marker. The h-BN domains are hardly observed. In Figure 4, panels f and g show the POM images on rotational angles of the sample for 0° and 90°, respectively (see Supporting Information, Figure S6, for details). The white- and green-dotted areas indicate the regions where h-BN domains were grown on the Pt (111) and (001) planes, respectively, as shown in Figure 4a. The colors of each h-BN domain, including the white- and green-dotted regions, were similarly changed as a function of the polarized angle, indicating that the h-BN has a similar orientation within the domains. However, the POM image at higher magnification (Figure 4h) reveals a slightly different color contrast even within the h-BN domain (II and III), indicating the formation of intradomains, whereas domain I shows the same color. A similar result has been reported for polycrystalline graphene on Cu foil.[45] At the initial growth stage, many h-BN islands were nucleated on the Pt (111) plane (see Supporting Information, Figure S7). The lattice

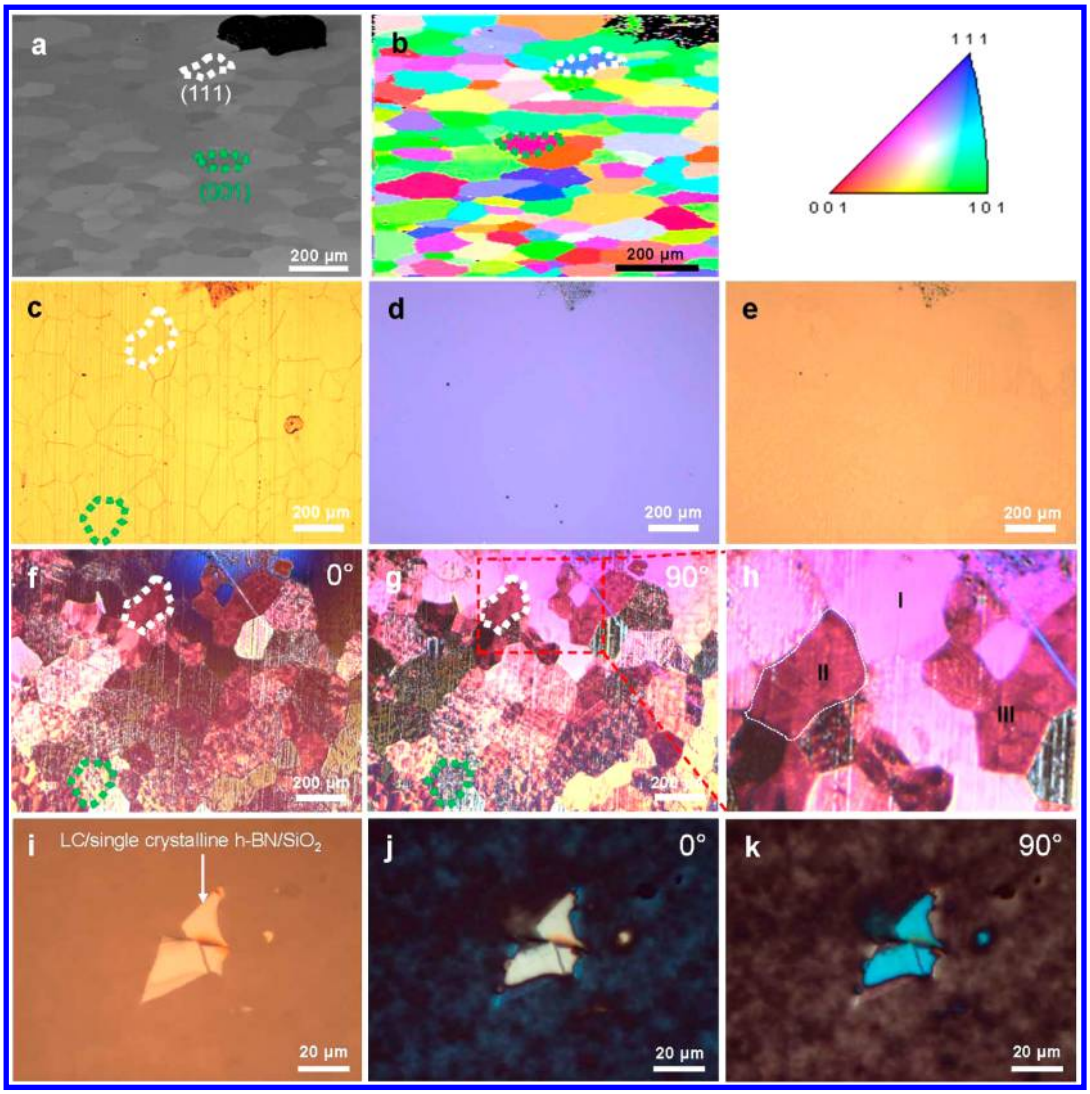

Figure 4. The effect of Pt lattice orientation for h-BN growth and visualization of h-BN domains. (a) SEM image of h-BN on Pt foil. The white- and green-dotted lines indicate the Pt (111) and Pt (001) region, respectively. The black region on the top is silver-paste marker. (b) EBSD image of the same region as (a) and the EBSD legend. (c) Optical image of the same region as (a). (d) Optical image of h-BN transferred onto SiO_2/Si. (e) Optical image of LC-coated h-BN on a SiO_2/Si. (f and g) POM images on rotational angles of the sample for 0° and 90° of the same region as (d). (h) POM image at a higher magnification of the box in (g). (i) Optical image of LC-coated single crystalline h-BN flake transferred onto SiO_2/Si. (j and k) POM images for the rotation angle of 0° and 90° of the same region as (i).

mismatch between h-BN and Pt (111) is ~10%, which is attributed to intradomain formation. Nonetheless, the exact correlation between the crystallinity of the h-BN and the lattice orientation of Pt still needs to be studied further.

To confirm the validity of LC-assisted POM method on h-BN, the single crystalline h-BN flake obtained from the mechanical exfoliation was characterized by the same method. Figure 4i shows the optical image of the single crystalline h-BN flake coated with the nematic LC. The color of the single crystalline h-BN flake was uniform and changed with the rotation angles of 0° and 90° in the POM images, as shown in Figure 4j,k. This indicates that the flake is a single-domain, in contrast with the observed polycrystalline domains (see Supporting Information, Figure S8, for details). The domain size of h-BN can be directly measured in the POM image. By comparing the Pt and h-BN domains, (i) the orientation of the h-BN domain is largely affected by the underlying Pt lattice orientation. The misalignment angle of the h-BN intradomains within each h-BN domain is small compared to the misalignment with other h-BN domains grown at a different Pt lattice orientation. (ii) Some h-BN domains show a single-crystallinity within the domain, which implies the synthesis of a single crystalline h-BN on a specific Pt lattice orientation.

The monolayer h-BN in this work was synthesized at a total pressure of 0.1 Torr, under a hydrogen and borazine atmosphere, at a flow rate of 10 and 0.2 sccm. In our CVD, the lower limit of the flow rate of the precursor was 0.2 sccm. At this lowest flow rate, the

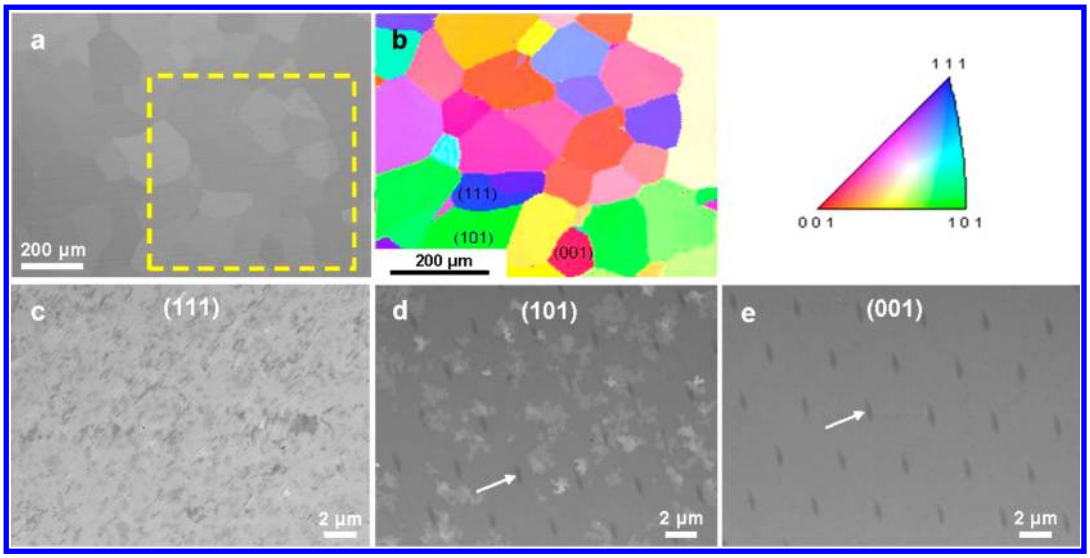

Figure 5. The pressure effect for h-BN growth on Pt foil. (a) SEM image of Pt foil after h-BN growth at a pressure of 0.5 Torr. (b) EBSD mapping image corresponding to the yellow-dashed box in (a) and the EBSD legend. (c−e) SEM images of the Pt (111), Pt (101), and Pt (001) planes after EBSD mapping. The black dots indicated by white arrow in (d) and (e) were induced by the electron-beam damage during the EBSD mapping.

monolayer h-BN film on Pt foil was achieved. To understand the effect of the amount of precursors, the total pressure at the lowest flow rate of the precursor (0.2 sccm) was controlled by using a needle valve.[46] The SEM image in Figure 5a shows the polycrystalline Pt surface after growing the h-BN film at a total pressure of 0.5 Torr. Figure 5b is the EBSD mapping image of Pt corresponding to the yellow-dotted box in Figure 5a, which includes the Pt (111), Pt (101), and Pt (001) planes. The SEM images in Figure 5c−e show the h-BN films grown on the Pt (111), Pt (101), and Pt (001) planes, respectively. Thick h-BN film was obtained on a Pt (111) plane (Figure 5c), and h-BN flakes on a thin h-BN film were synthesized on Pt (101) planes (Figure 5d) (see Supporting Information, Figure S9). Interestingly, a thin h-BN film, without the additional h-BN flakes, was grown on a Pt (001) plane (Figure 5e). The h-BN wrinkles were clearly observed on a Pt (001) plane (see Supporting Information, Figure S10). The black dots indicated by white arrows in Figure 5d,e were induced by the electron-beam damage during the EBSD mapping, supporting the idea that a thin h-BN film was grown in those regions; something which is markedly distinguished from the thick h-BN film grown on Pt (111) planes (Figure (5c). The different growth behavior on Pt lattice orientations is not well-understood here. It could be attributed to the fact that the higher catalytic effect of the Pt (111) plane, in comparison to other planes,[47] leads to more efficient decomposition of the borazine precursors and, as a consequence, thick h-BN film is grown there.

CONCLUSION

We have synthesized a large-area monolayer h-BN onto a Pt foil with borazine precursor by using CVD. The h-BN film was synthesized with the surface-mediated growth mechanism, which was confirmed by the different cooling rate experiment. To obtain a monolayer h-BN on Pt foil, the growth should be carried out under a pressure lower than 100 mTorr. The resulting monolayer h-BN was polycrystalline, as was confirmed by the nematic LC-assisted POM method and the SAED pattern in TEM. In addition, the orientation of the h-BN domains was largely confined by the underlying Pt lattice orientation. At high pressure, a thick h-BN film was preferentially grown on Pt (111), whereas the thin h-BN film was grown on Pt (001). The possible explanation for this is that the catalytic effect of the Pt (111) surface is higher than that of the Pt (001) surface due to the higher density of the Pt atoms, leading to a more efficient decomposition of the borazine precursor. By understanding how to grow large-area monolayer h-BN, we can ignite research related to the control of high-quality h-BN film growth, which can be applied to vertical quantum tunneling devices and further used in growth templates for numerous heterostructures such as GaN, MoS_2, and graphene.

METHODS

Smooth Surface and Grain Growth of Platinum Foil. To remove any impurities on the Pt surface, a Pt foil (thickness of 0.1 mm, Goodfellow) with a size of 2 × 5 cm^2 was washed with acetone and 2-propanol after sonication in acetone and Ni etchant (Nickel etchant TFB, Transene) for 5 and 2 min, respectively.

The solvent on the Pt surface was then blown away with N_2 gas. To obtain a smooth surface and grow the Pt grains, Pt foil was preannealed at 1100 °C for 2 h under a hydrogen atmosphere at a rate of 100 sccm before h-BN growth. After preannealing, the Pt grains in a size of 50−200 μm were observed, with the Pt foil presenting a very smooth surface (see Supporting Information, Figure S11).

Synthesis of h-BN. To grow an h-BN film, a Pt foil was placed at the center of a quartz tube with a diameter of one inch. The furnace was then ramped up to 1100 °C for 30 min under a flow of 10 sccm of H_2 gas and maintained there for 15 min in order to stabilize the temperature. A Pt foil with a size of 2×5 cm^2 was synthesized for 20 min with borazine and hydrogen at a flow rate of 0.2 and 10 sccm, respectively (total pressure was 0.1 Torr). A hydrogen line was connected to the bubbler as a carrier gas. The flow of 0.2 sccm, as a precursor, includes the hydrogen gas and borazine vapor. Therefore, the partial pressure of the borazine was less than 10 mTorr, as measured by the convectron gauge in this work. Finally, the furnace heat was turned down with various cooling rates until it reached room temperature. To study the effect of the amount of borazine used, the total pressure was controlled by the needle valve that was installed between chamber and pump.

Transfer of h-BN onto Flat Substrate and TEM Grid. Because the foil is Pt, which is a noble metal and difficult to be dissolved by the etchant, we used the bubbling-based transfer method. First, h-BN/Pt was spin-coated with PMMA (C4, Micro Chem) at 1000 rpm for 1 min and then dried in the oven at 80 °C for 30 min. After the drying step, the PMMA/h-BN/Pt was immersed in an aqueous solution of 0.1 M NaOH and used as a cathode. PMMA/h-BN was detached from Pt foil by applying a voltage of 10 V. After it was rinsed thrice with DI water, it was transferred onto target substrates and dried with vertical stand in the oven at 80 °C for an hour. The PMMA on the h-BN was removed by acetone. To analyze the morphology by AFM, thermal annealing was carried out at 400 °C for 2 h with a flow rate of 200 sccm for hydrogen and 200 sccm for Ar. Through this process, residues of PMMA were removed and adhesion between h-BN and SiO_2 was improved. To study TEM, the PMMA/h-BN layer was transferred onto the PELCO Holey Silicon Nitride support film with 2.5 μm holes (TedPella, Inc.). To prevent tearing or loss of h-BN on the TEM grid, the PMMA was removed only by thermal oxidation, at 500 °C, for 3 h, with a flow of 500 sccm (and 19 sccm) for Ar (and O_2) in a basal vacuum of 5×10^{-2} Torr, without acetone treatment.[26,33]

Characterization. A field-emission SEM (JSM7000F, JEOL) was used to observe the surface morphology and collect EBSD. POM (Axio Imager 2, ZEISS) was used to observe the texture of LC molecules (5CB, E.Merck) aligned on the h-BN/SiO_2. For the comparison, the same experiment was carried out on a single crystal h-BN purchased from the 2D semiconductors. Micro-Raman spectroscopy (RM1000-Invia, Renishaw, 532 nm) and Confocal Raman spectroscopy (CRM200, WITec, 532 nm) were used to observe the thickness and quality of the h-BN. The thickness and roughness of the h-BN on the SiO_2 substrate was measured using AFM (SPA 400, SEIKO). TEM (JEM ARM 200F, JEOL, 80 kV) and XPS (ESCA2000, VG Microtech) were used to characterize the atomic structure and elements of h-BN, respectively.

Conflict of Interest: The authors declare no competing financial interest.

Supporting Information Available: AFM, SEM, atomic-resolution TEM, POM, and EBSD images; XPS and Raman spectra. This material is available free of charge via the Internet at http://pubs.acs.org.

Acknowledgment. This work was supported by the Institute for Basic Science (IBS) in Korea. K.K.K. acknowledges the support from the Leading Foreign Research Institute Recruitment Program through the National Research Foundation of Korea (NRF) funded by the Ministry of Education, Science and Technology (MEST) (No.2012-00109). J.K. acknowledges the support through the STC Center for Integrated Quantum Materials from NSF (US) grant DMR-1231319. S.M.K. acknowledges the Korea Institute of Science and Technology (KIST) Institutional Program.

REFERENCES AND NOTES

1. Watanabe, K.; Taniguchi, T.; Kanda, H. Direct-Bandgap Properties and Evidence for Ultraviolet Lasing of Hexagonal Boron Nitride Single Crystal. *Nat. Mater.* **2004**, *3*, 404–409.
2. Dean, C. R.; Young, A. F.; Meric, I.; Lee, C.; Wang, L.; Sorgenfrei, S.; Watanabe, K.; Taniguchi, T.; Kim, P.; Shepard, K. L.; *et al.* Boron Nitride Substrates for High-Quality Graphene Electronics. *Nat. Nanotechnol.* **2010**, *5*, 722–726.
3. Lee, K. H.; Shin, H. J.; Lee, J.; Lee, I. Y.; Kim, G. H.; Choi, J. Y.; Kim, S. W. Large-Scale Synthesis of High-Quality Hexagonal Boron Nitride Nanosheets for Large-Area Graphene Electronics. *Nano Lett.* **2012**, *12*, 714–718.
4. Yang, W.; Chen, G.; Shi, Z.; Liu, C. C.; Zhang, L.; Xie, G.; Cheng, M.; Wang, D.; Yang, R.; Shi, D.; *et al.* Epitaxial Growth of Single-Domain Graphene on Hexagonal Boron Nitride. *Nat. Mater.* **2013**, *12*, 792–797.
5. Giovannetti, G.; Khomyakov, P. A.; Brocks, G.; Kelly, P. J.; van den Brink, J. Substrate-Induced Band Gap in Graphene on Hexagonal Boron Nitride: *Ab Initio* Density Functional Calculations. *Phys. Rev. B* **2007**, *76*, 073103.
6. Hunt, B.; Sanchez-Yamagishi, J. D.; Young, A. F.; Yankowitz, M.; LeRoy, B. J.; Watanabe, K.; Taniguchi, T.; Moon, P.; Koshino, M.; Jarillo-Herrero, P.; *et al.* Massive Dirac Fermions and Hofstadter Butterfly in a van der Waals Heterostructure. *Science* **2013**, *340*, 1427–1430.
7. Zhi, C.; Bando, Y.; Tang, C.; Kuwahara, H.; Golberg, D. Large-Scale Fabrication of Boron Nitride Nanosheets and Their Utilization in Polymeric Composites with Improved Thermal and Mechanical Properties. *Adv. Mater.* **2009**, *21*, 2889–2893.
8. Liu, Z.; Gong, Y.; Zhou, W.; Ma, L.; Yu, J.; Idrobo, J. C.; Jung, J.; MacDonald, A. H.; Vajtai, R.; Lou, J.; *et al.* Ultrathin High-Temperature Oxidation-Resistant Coatings of Hexagonal Boron Nitride. *Nat. Commun.* **2013**, *4*, 2541.
9. Lindsay, L.; Broido, D. A. Enhanced Thermal Conductivity and Isotope Effect in Single-Layer Hexagonal Boron Nitride. *Phys. Rev, B* **2011**, *84*, 155421.
10. Li, L. H.; Cervenka, J.; Watanabe, K.; Taniguchi, T.; Chen, Y. Strong Oxidation Resistance of Atomically Thin Boron Nitride Nanosheets. *ACS Nano* **2014**, *8*, 1457–1462.
11. Chiang, T. H.; Hsieh, T. E. A Study of Encapsulation Resin Containing Hexagonal Boron Nitride (hBN) as Inorganic Filler. *J. Inorg. Organomet. Polym.* **2006**, *16*, 175–183.
12. Zhu, H.; Li, Y.; Fang, Z.; Xu, J.; Cao, F.; Wan, J.; Preston, C.; Yang, B.; Hu, L. Highly Thermally Conductive Papers with Percolative Layered Boron Nitride Nanosheets. *ACS Nano* **2014**, *8*, 3606–3613.
13. Nagashima, A.; Tejima, N.; Gamou, Y.; Kawai, T.; Oshima, C. Electronic Dispersion-Relations of Monolayer Hexagonal Boron-Nitride Formed on the Ni(111) Surface. *Phys. Rev. B* **1995**, *51*, 4606–4613.
14. Nagashima, A.; Tejima, N.; Gamou, Y.; Kawai, T.; Oshima, C. Electronic-Structure of Monolayer Hexagonal Boron-Nitride Physisorbed on Metal-Surfaces. *Phys. Rev. Lett.* **1995**, *75*, 3918–3921.
15. Nagashima, A.; Tejima, N.; Gamou, Y.; Kawai, T.; Oshima, C. Electronic States of Monolayer Hexagonal Boron Nitride Formed on the Metal Surfaces. *Surf. Sci.* **1996**, *357*, 307–311.
16. Corso, M.; Greber, T.; Osterwalder, J. h-BN on Pd(110): A Tunable System for Self-Assembled Nanostructures? *Surf. Sci.* **2005**, *577*, L78–L84.
17. Corso, M.; Auwärter, W.; Muntwiler, M.; Tamai, A.; Greber, T.; Osterwalder, J. Boron Nitride Nanomesh. *Science* **2004**, *303*, 217–220.
18. Hemmi, A.; Bernard, C.; Cun, H.; Roth, S.; Klockner, M.; Kalin, T.; Weinl, M.; Gsell, S.; Schreck, M.; Osterwalder, J.; *et al.* High Quality Single Atomic Layer Deposition of Hexagonal Boron Nitride on Single Crystalline Rh(111) Four-Inch Wafers. *Rev. Sci. Instrum.* **2014**, *85*, 035101–035104.

19. Müller, F.; Hüefner, S.; Sachdev, H.; Laskowski, R.; Blaha, P.; Schwarz, K. Epitaxial Growth of Hexagonal Boron Nitride on Ag(111). *Phys. Rev. B* **2010**, *82*, 113406.
20. Müller, F.; Grandthyll, S. Monolayer Formation of Hexagonal Boron Nitride on Ag(001). *Surf. Sci.* **2013**, *617*, 207–210.
21. Kim, K. K.; Kim, S. M.; Lee, Y. H. A New Horizon for Hexagonal Boron Nitride Film. *J. Korean Phys. Soc.* **2014**, *64*, 1605–1616.
22. Shi, Y.; Hamsen, C.; Jia, X.; Kim, K. K.; Reina, A.; Hofmann, M.; Hsu, A. L.; Zhang, K.; Li, H.; Juang, Z. Y.; *et al.* Synthesis of Few-Layer Hexagonal Boron Nitride Thin Film by Chemical Vapor Deposition. *Nano Lett.* **2010**, *10*, 4134–4139.
23. Lee, Y. H.; Liu, K. K.; Lu, A. Y.; Wu, C. Y.; Lin, C. T.; Zhang, W.; Su, C. Y.; Hsu, C. L.; Lin, T. W.; Wei, K. H.; *et al.* Growth Selectivity of Hexagonal-Boron Nitride Layers on Ni with Various Crystal Orientations. *Rsc. Adv.* **2012**, *2*, 111–115.
24. Gibb, A. L.; Alem, N.; Chen, J. H.; Erickson, K. J.; Ciston, J.; Gautam, A.; Linck, M.; Zettl, A. Atomic Resolution Imaging of Grain Boundary Defects in Monolayer Chemical Vapor Deposition-Grown Hexagonal Boron Nitride. *J. Am. Chem. Soc.* **2013**, *135*, 6758–6761.
25. Orofeo, C. M.; Suzuki, S.; Kageshima, H.; Hibino, H. Growth and Low-Energy Electron Microscopy Characterization of Monolayer Hexagonal Boron Nitride on Epitaxial Cobalt. *Nano Res.* **2013**, *6*, 335–347.
26. Orofeo, C. M.; Suzuki, S.; Hibino, H. Ultrathin Chemical Vapor Deposition (CVD)-Grown Hexagonal Boron Nitride as a High-Quality Dielectric for Tunneling Devices on Rigid and Flexible Substrates. *J. Phys. Chem. C* **2014**, *118*, 3340–3346.
27. Song, L.; Ci, L.; Lu, H.; Sorokin, P. B.; Jin, C.; Ni, J.; Kvashnin, A. G.; Kvashnin, D. G.; Lou, J.; Yakobson, B. I.; *et al.* Large Scale Growth and Characterization of Atomic Hexagonal Boron Nitride Layers. *Nano Lett.* **2010**, *10*, 3209–3215.
28. Kim, K. K.; Hsu, A.; Jia, X.; Kim, S. M.; Shi, Y.; Hofmann, M.; Nezich, D.; Rodriguez-Nieva, J. F.; Dresselhaus, M.; Palacios, T.; *et al.* Synthesis of Monolayer Hexagonal Boron Nitride on Cu Foil Using Chemical Vapor Deposition. *Nano Lett.* **2012**, *12*, 161–166.
29. Kim, K. K.; Hsu, A.; Jia, X.; Kim, S. M.; Shi, Y.; Dresselhaus, M.; Palacios, T.; Kong, J. Synthesis and Characterization of Hexagonal Boron Nitride Film as a Dielectric Layer for Graphene Devices. *ACS Nano* **2012**, *6*, 8583–8590.
30. Han, J.; Lee, J. Y.; Kwon, H.; Yeo, J. S. Synthesis of Wafer-Scale Hexagonal Boron Nitride Monolayers Free of Aminoborane Nanoparticles by Chemical Vapor Deposition. *Nanotechnology* **2014**, *25*, 145604.
31. Kim, G.; Jang, A. R.; Jeong, H. Y.; Lee, Z.; Kang, D. J.; Shin, H. S. Growth of High-Crystalline, Single-Layer Hexagonal Boron Nitride on Recyclable Platinum Foil. *Nano Lett.* **2013**, *13*, 1834–1839.
32. Gao, Y.; Ren, W. C.; Ma, T.; Liu, Z.; Zhang, Y.; Liu, W. B.; Ma, L. P.; Ma, X.; Cheng, H. M. Repeated and Controlled Growth of Monolayer, Bilayer and Few-Layer Hexagonal Boron Nitride on Pt Foils. *ACS Nano* **2013**, *7*, 5199–5206.
33. Garcia, A. G. F.; Neumann, M.; Amet, F.; Williams, J. R.; Watanabe, K.; Taniguchi, T.; Goldhaber-Gordon, D. Effective Cleaning of Hexagonal Boron Nitride for Graphene Devices. *Nano Lett.* **2012**, *12*, 4449–4454.
34. Gorbachev, R. V.; Riaz, I.; Nair, R. R.; Jalil, R.; Britnell, L.; Belle, B. D.; Hill, E. W.; Novoselov, K. S.; Watanabe, K.; Taniguchi, T.; *et al.* Hunting for Monolayer Boron Nitride: Optical and Raman Signatures. *Small* **2011**, *7*, 465–468.
35. Arenal, R.; Ferrari, A. C.; Reich, S.; Wirtz, L.; Mevellec, J. Y.; Lefrant, S.; Rubio, A.; Loiseau, A. Raman Spectroscopy of Single-Wall Boron Nitride Nanotubes. *Nano Lett.* **2006**, *6*, 1812–1816.
36. Huang, J. Y.; Yasuda, H.; Mori, H. HRTEM and EELS Studies on The Amorphization of Hexagonal Boron Nitride Induced by Ball Milling. *J. Am. Ceram. Soc.* **2000**, *83*, 403–409.
37. Kotakoski, J.; Jin, C. H.; Lehtinen, O.; Suenaga, K.; Krasheninnikov, A. V. Electron Knock-On Damage in Hexagonal Boron Nitride Monolayers. *Phys. Rev. B* **2010**, *82*, 113404.
38. Li, X. S.; Cai, W.; Colombo, L.; Ruoff, R. S. Evolution of Graphene Growth on Ni and Cu by Carbon Isotope Labeling. *Nano Lett.* **2009**, *9*, 4268–4272.
39. Li, X. S.; Cai, W.; An, J.; Kim, S.; Nah, J.; Yang, D.; Piner, R.; Velamakanni, A.; Jung, I.; Tutuc, E.; *et al.* Large-Area Synthesis of High-Quality and Uniform Graphene Films on Copper Foils. *Science* **2009**, *324*, 1312–1314.
40. Yu, Q.; Lian, J.; Siriponglert, S.; Li, H.; Chen, Y. P.; Pei, S. S. Graphene Segregated on Ni Surfaces and Transferred to Insulators. *Appl. Phys. Lett.* **2008**, *93*, 113103.
41. Massalski, T. B.; Okamoto, H. *Binary Alloy Phase Diagrams*, 2nd ed.; ASM International: Materials Park, OH, 1990.
42. Kang, B. J.; Mun, J. H.; Hwang, C. Y.; Cho, B. J. Monolayer Graphene Growth on Sputtered Thin Film Platinum. *J. Appl. Phys.* **2009**, *106*, 104309.
43. Paszkowicz, W.; Pelka, J. B.; Knapp, M.; Szyszko, T.; Podsiadlo, S. Lattice Parameters and Anisotropic Thermal Expansion of Hexagonal Boron Nitride in the 10−297.5 K Temperature Range. *Appl. Phys. A: Mater. Sci. Process.* **2002**, *75*, 431–435.
44. Kim, D. W.; Kim, Y. H.; Jeong, H. S.; Jung, H. T. Direct Visualization of Large-Area Graphene Domains and Boundaries by Optical Birefringency. *Nat. Nanotechnol.* **2012**, *7*, 29–34.
45. Son, J. H.; Baeck, S. J.; Park, M. H.; Lee, J. B.; Yang, C. W.; Song, J. K.; Zin, W. C.; Ahn, J. H. Detection of Graphene Domains and Defects Using Liquid Crystals. *Nat. Commun.* **2014**, *5*, 3484.
46. Sun, Z.; Raji, A. R. O.; Zhu, Y.; Xiang, C.; Yan, Z.; Kittrel, C.; Samuel, E. L. G.; Tour, J. M. Large-Area Bernal-Stacked Bi-, Tr-, and Tetralayer Graphene. *ACS Nano* **2012**, *6*, 9790–9796.
47. Gao, T.; Xie, S.; Gao, Y.; Liu, M.; Chen, Y.; Zhang, Y.; Liu, Z. Growth and Atomic-Scale Characterizations of Graphene on Multifaceted Textured Pt Foils Prepared by Chemical Vapor Deposition. *ACS Nano* **2011**, *5*, 9194–9201.